TENSILE BEHAVIOR OF REPAIRED THERMOPLASTIC COMPOSITE JOINTS THROUGH ULTRASONIC WELDING

W. Li^a and G. Palardy^a*

^a Department of Mechanical and Industrial Engineering, Louisiana State University
3261 Patrick F. Taylor Hall
Baton Rouge, LA 70803, United States

ABSTRACT

Joints in assembled thermoplastic composite (TPC) structures are susceptible to damage during their service life and threaten their structural integrity. It is crucial to develop effective repair methods to enable the recovery of structural strength and improve repair quality. In this regard, as assembly of TPC joints through welding is gaining importance, there is a need to assess their potential for repairability. In this work, repair of ultrasonically welded joints with multifunctional nanocomposite films is investigated. Herein, single lap shear joints were repaired by welding nanocomposite films (multi-walled carbon nanotube/polypropylene (MWCNT/PP)) sandwiched between glass fiber/polypropylene (GF/PP) adherends. Mechanical properties under tensile loading and the effect of repeated repair operations (three cycles) on the lap shear strength (LSS) were investigated, and a comparison was made between MWCNT/PP film repaired specimens and control specimens (pure PP film). The PP film repair indicated significant potential to reinstate LSS with 94.5 %, 89.4 %, and 86.7 % of initial specimen LSS for each cycle, while the strength could be partially restored with MWCNT/PP film. Moreover, during mechanical testing, electrical resistance measurements at the welded interface provided in-situ real-time structural health monitoring (SHM) for damage mechanisms of repaired GF/PP joints, in addition to fractography analyses after repair cycles. Overall, the repair capability of the ultrasonic-assisted technique for TPC joints was confirmed in this study and MWCNT-based nanocomposite films showed potential for real-time damage detection of repaired joints.

Keywords: Thermoplastic composites, repair, ultrasonic welding Corresponding author: Genevieve Palardy (gpalardy@lsu.edu)

1. INTRODUCTION

Fiber-reinforced polymer (FRP) composites have been attracting the interest of academia and industry due to their high specific strength and stiffness, light weight, excellent corrosion resistance, fatigue resistance, and ease of complex structure designs [1, 2]. Among these composites, thermoplastic composites (TPCs) have been increasingly used in a variety of fields, such as aerospace, automotive, maritime, wind energy, biomedical, and oil & gas, where strength and weight are of paramount importance [3]. Consequently, this demand drives an ever-growing development of larger and more integrated composite structures.

Copyright 2023. Used by the Society of the Advancement of Material and Process Engineering with permission.

SAMPE Conference Proceedings. Seattle, WA, April 17-20, 2023. Society for the Advancement of Material and Process Engineering – North America. However, existing composite structures are susceptible to damage during service under loads, threatening their integrity. It is critical to repair or replace current composite structures to extend their life by restoring strength. Repair is generally low-cost and can provide partial strength recovery, whereas replacement is usually adopted when structures suffer severe damages [2, 4, 5]. The most common repair techniques used for composite structures, predominantly applied to thermoset composites, are resin injection repair, mechanical fasteners, bonded repair (including scarf repair and patch repair), and mendable polymer repair. The former injects liquid resin into the delaminated region via drilled holes; however, during this process, the delamination can easily become contaminated by the environment [6, 7]. Although mechanical fastener repair is more reliable and effective than injecting epoxy resin, this technique can only restore strength to a limited extent. For example, the reduced compression failure strength of composite laminates was restored from 64.5 %, 57.3 %, and 39.5 % to 79.2 %, 70.7 % and 49.5 % with impact damage of different energy levels, respectively [6]. Of all repair techniques, bonded repair is most widely researched and used [2, 4, 5, 8-10]. Bhatia et al. [8] and Sahoo et al. [2] both investigated the influence of stacking sequence of parent laminate and the stacking sequence of patches on the repair behavior of laminates under tensile fatigue loading and tensile loading, respectively. In [4], Ji et al. designed a bi-adhesive repair approach and evaluated the damage behavior of different repaired composites subjected to three-point bending using acoustic emission (AE) and microcomputed tomography (CT) methods. Nevertheless, most bonded repairs can only be performed once for traditional composites. Toward this end, researchers, such as Loh et al. [7, 11] and Li et al. [12] studied the incorporation of thermoplastic particles in laminates or adhesively bonded joints as a repair agent to heal cracks through heating the damaged areas.

To the authors' knowledge, until now, there is limited research available for repair of TPC joints. As TPCs are suitable for fusion bonding (welding), this method can be leveraged for repair [13]. Among the main welding methods, ultrasonic welding (USW) is one of the most attractive techniques. It uses high-frequency and low-amplitude vibrations to generate heat between adherends through surface friction and viscoelastic heating, while pressure is applied by a sonotrode. Over the past few years, USW of TPCs has been studied, mostly as a joining technique [14-20]. It is expected that welded joints can be repaired by re-welding broken components, or using assistive heating methods for localized repair, such as resistance or induction heating [21]. Previous work explored the use of multi-walled carbon nanotube (MWCNT)-based multifunctional films to enable several functions: 1) heat generation during USW, 2) structural health monitoring (SHM) through electrical resistance changes, 3) resistance heating-assisted disassembly of welded TPC joints, and 4) repair through USW [22-27]. In this study, the last function will be investigated by assessing effectiveness of ultrasonic-assisted repair.

Therefore, the main goal of this work is to quantify strength recovery after USW-assisted repair and to evaluate damage monitoring of repaired TPC joints under tensile loading. In this study, fully broken glass fiber/polypropylene (GF/PP) joints were repaired with pure PP and MWCNT-based nanocomposite films for three repair cycles using USW, followed by an investigation of their tensile behavior. In addition, failure modes were compared to provide a deeper understanding of tensile behavior after repair operations. Finally, the damage sensing capability of MWCNT-based nanocomposite films for repaired joints was evaluated.

2. EXPERIMENTAL METHODS

2.1. Materials and sample preparations

Nanocomposite materials used in this study were commercially-available 15 wt% MWCNT/PP pellets produced by twin-screw extrusion from Cheap Tubes Inc. (Grafton, VT, USA). They were selected for manufacturing multifunctional films in this study, based on our previous research [26]. Pure PP films, as a control group, were fabricated from PP pellets (Goodfellow, Coraopolis, PA, USA), with a granule size of 5 mm and a melt flow of 6 g/min. Both types of films were made through compression molding using a laboratory hot press (DAKE, Grand Haven, MI, USA) through consolidation at 180 °C for 15 min, under a pressure of 0.8 MPa. During the compression process, stainless-steel shims were used to control the final thickness of the films to 0.5 mm. The laminates used as adherends were made from 0.33 mm-thick unidirectional (UD) GF/PP prepregs (IE 6030) with a 60 % fiber volume fraction supplied by Avient (formerly PolyOne, Avon Lake, OH, USA). Eight 254 mm × 254 mm GF/PP prepreg layers were stacked in a [0]₈ configuration. The stacked prepregs were first bonded using a handheld ultrasonic welder to prevent them from moving during processing and then consolidated at 180 °C for 15 min under a pressure of 1 MPa by a hot press, followed by cooling down to room temperature overnight. Obtained laminates had a nominal thickness of 1.8 mm. Adherends of required dimensions (101.6 mm × 25.4 mm) were cut from the laminates using a diamond water saw (PICO 155 Precision Saw, Pace Technologies, Tucson, AZ, USA) according to ASTM D1002. Their long side was parallel to the direction of the glass fibers.

2.2. Ultrasonic welding and repair technique

GF/PP adherends were joined in a single lap configuration using a Dynamic 3000 ultrasonic welder (Rinco Ultrasonics, Danbury, CT, USA) with a 20 kHz frequency and a maximum power of 3000 W. As shown in Figure 1, a nanocomposite film, as an energy director (ED), was sandwiched between two GF/PP adherends with an overlap of 12.7 mm × 25.4 mm and the upper adherend was supported by a GF/PP specimen with the same thickness as the lower one, allowing for vertical displacement when the ED was squeezed out during welding. In addition, both adherends were fixed by a pair of customized clamps with a 25.4 mm-wide groove to allow their movement only in the vertical direction. The vibration was amplified through a booster gain of 1:1.5 and a sonotrode gain of 1:3.85. A 1000 N welding force and 38.1 μm vibration amplitude were applied to join those two adherends, followed by a consolidation step with a force of 1000 N for 4000 ms. This welding process was controlled by the vertical displacement of the sonotrode equal to 60 % travel (i.e., 60 % of initial nanocomposite film thickness). As a reference, GF/PP adherends were also welded with PP films. The single lap joint (SLJ) samples in this study were named PP-GF/PP and MWCNT-GF/PP SLJs.

Ultrasonic welding was used to repair the broken TPC SLJs. In this study, three repair cycles were performed to investigate the feasibility of ultrasonic-assisted repair through evaluating strength recovery and failure modes. After breaking SLJs under tension, the excess films squeezed out of the interface under pressure were removed to improve the flatness of repaired surfaces and eliminate their effect on repair operations. A 0.5 mm-thick PP film or MWCNT/PP film was then placed between the two broken adherends and the vertical displacement of the sonotrode was controlled by a 60 % travel value. Furthermore, all repair parameters remained the same as the initial joint manufacturing process.

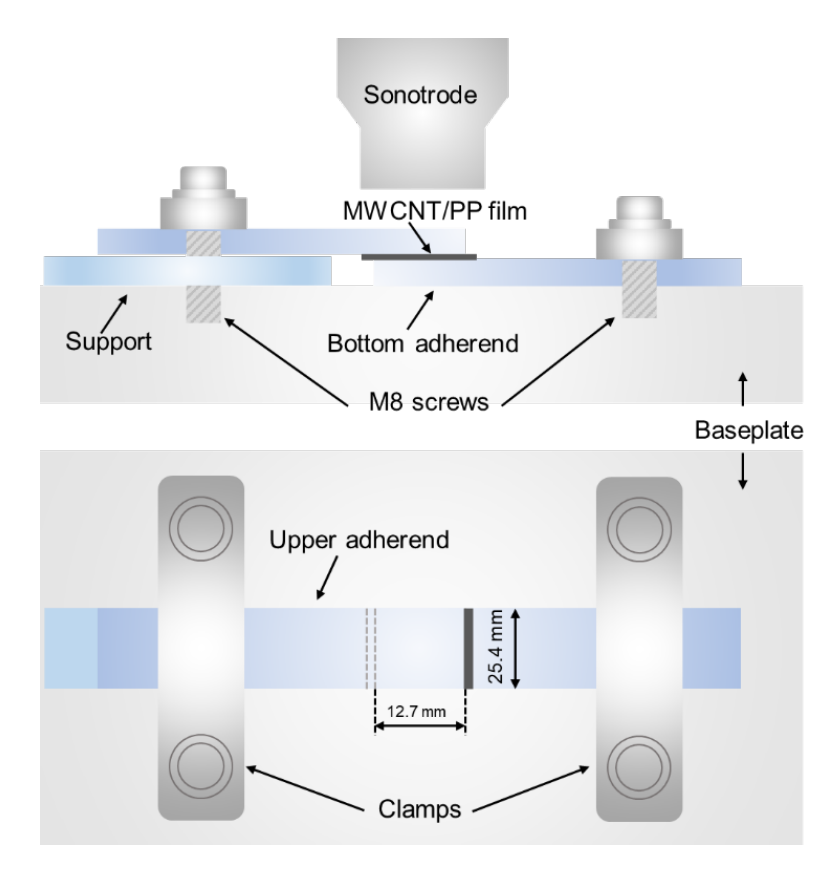


Figure 1. Schematic of ultrasonic welding setup.

2.3. Tensile tests and failure modes

After each repair cycle, the tensile behavior of the joints was characterized with a 50 kN testing machine from TestResources, Model 313 to quantify their strength recovery with respect to the initial joints. Before performing tensile tests, squeezed out films at the edges of the repaired SLJs were removed. The distance between the two hydraulic square grips was set to 60 mm and the central line of the upper and lower grips was aligned with the welding line. Subsequently, a load was applied to the joint with a crosshead speed of 1.3 mm/min until ultimate failure according to ASTM D1002. Lap shear strength (LSS) was then calculated based on the failure load and joint area. At least five specimens were tested for each repair cycle to ensure repeatability of the failure mechanisms.

To investigate the effect of repeated repair operations on failure modes, visual inspection was first used to observe the fracture surfaces for repaired PP-GF/PP and MWCNT-GF/PP SLJs. In addition, to better understand failure mechanisms after repair, the fracture surfaces were further observed with a focused ion beam (FIB) high-resolution field emission gun scanning electron microscope (FEI QUANTA 3D FEG FIB/SEM). Before observation, fracture surfaces were spray-coated with gold under a vacuum of 1×10^{-1} mbar and 25 mA for 4 min to increase their conductivity, using a sputter coater (EMS550X).

2.4. Nanocomposite-based monitoring

To evaluate the damage sensing capability of nanocomposite films, even after repair cycles, repaired joints were monitored by electrical resistance measurements during tensile tests. Two

copper wires were sealed to the welding line interface (Figure 2) with silver paint (SPI #05002-AB), reducing the contact resistance and minimizing the effect of wire position with respect to the thin welding line. Painted specimens were dried overnight at room temperature. As shown in Figure 2, a 6 V voltage was supplied to the joint using a Keithley SourceMeter 2604B and its electrical resistance changes under tension were recorded by Keithley KickStart software. To prevent the increase of specimen temperature, a cooling fan was placed next to the joint. It is worth noting that before applying loading, electrical resistance was measured for 1 min to obtain the initial resistance (R_0), then the change of electrical resistance ($\Delta R/R_0$ (%)) was calculated. Since R_0 values exhibit significant deviation due to the experimental preparation variations and the measured electrical resistance may vary from one specimen to another under tension, it is common to use ($\Delta R/R_0$ (%)) as a comparison method. At least five specimens were tested to ensure the repeatability of the sensing response.

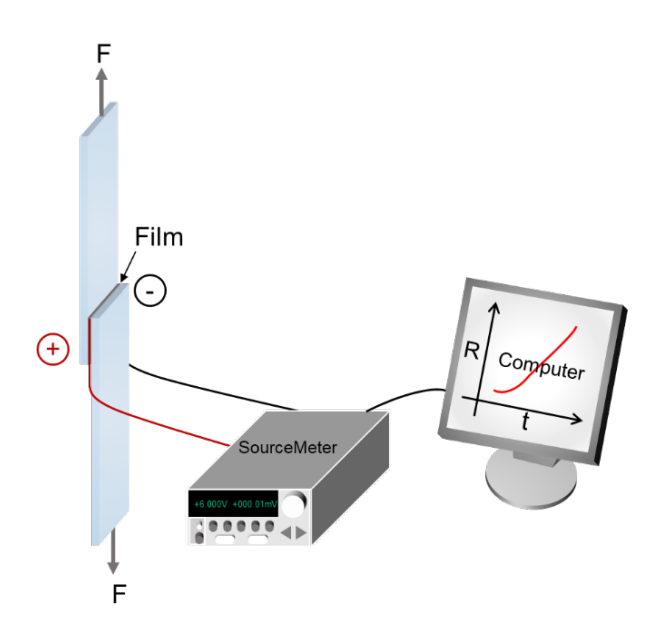


Figure 2. Schematic of tensile test and electrical resistance measurement setup for TPC joints repaired with MWCNT/PP films.

3. RESULTS AND DISCUSSIONS

3.1. Tensile behavior

First, tensile tests were performed on the initially welded joints to obtain the tensile behavior of PP-GF/PP and MWCNT-GF/PP SLJs. Figure 3 shows representative load-displacement curves of both initial joints with two samples for each case. Joints with MWCNT/PP films show a slightly higher stiffness and experience a shorter elongation at break compared to PP-GF/PP SLJs. This higher stiffness and lower elongation are caused by the incorporation of MWCNTs, creating a stiffer and more brittle nanocomposite polymer. On the other hand, due to the ductility of PP, it can extend more under tension, resulting in a longer displacement before failure. Furthermore, the stiffness of both types of joints decreases slightly in the second region (after elastic limitation) associated with the plastic deformation of the films.

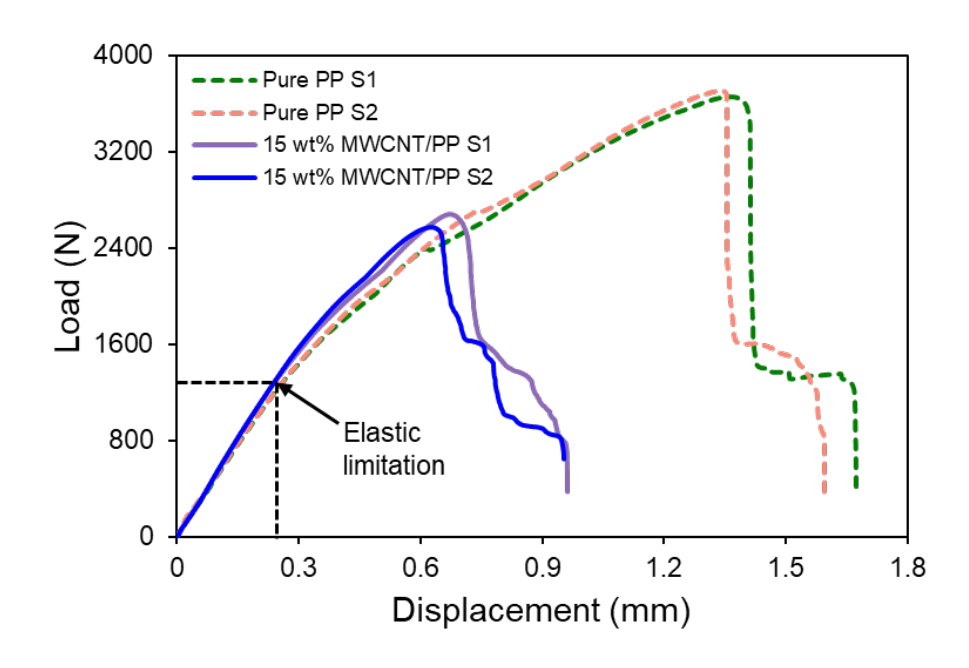


Figure 3. Representative load-displacement curves of initially welded PP-GF/PP and MWCNT-GF/PP SLJs. S1 and S2 represent the specimen number for each condition.

Following the initial mechanical tests, fully broken GF/PP joints were repaired using the developed repair technique described in Section 2.2. Subsequently, tensile tests were conducted again on the repaired joints to evaluate whether the ultrasonic-assisted repair was effective in re-bonding fractured adherends and recovering their strength. A series of failure loads and corresponding maximum displacements were obtained. Representative load-displacement curves after each repair operation, including the initial welds, are presented in Figure 4. All repaired PP-GF/PP SLJs (Figure 4a) have a higher failure load and extend more before failure, compared to MWCNT-GF/PP SLJs (Figure 4b). In addition, the failure loads and their corresponding displacements gradually decrease with the repair cycles for both cases (PP and MWCNT/PP films). The average LSS and standard deviation of all repaired joints for both film types are shown in Figure 5. Overall, the LSS recovery gradually decreases with increasing number of repair cycles for both cases, which indicates that ultrasonic-assisted repair is partially effective in re-bonding fractured surfaces. For PP films, 94.5 %, 89.4 %, and 86.7 % of LSS with respect to the initial joint were recovered after each repair cycle, respectively. MWCNT/PP films partially restore the strength to a lesser extent, possibly due to an increase in the thickness of welding line or fiber distortion, compared to PP films. Moreover, as the repair operation was repeated, the fracture surfaces became more uneven, potentially resulting in a non-uniform temperature distribution at the welding interface. Consequently, the extent of film melting varied. Lastly, as was previously observed in the literature [24, 28, 29], lower performance of nanocomposite films may be caused by their brittleness, compared to PP films. Overall, it was observed that PP films were effective in repairing fractured GF/PP adherends, while MWCNT/PP films were partially effective.

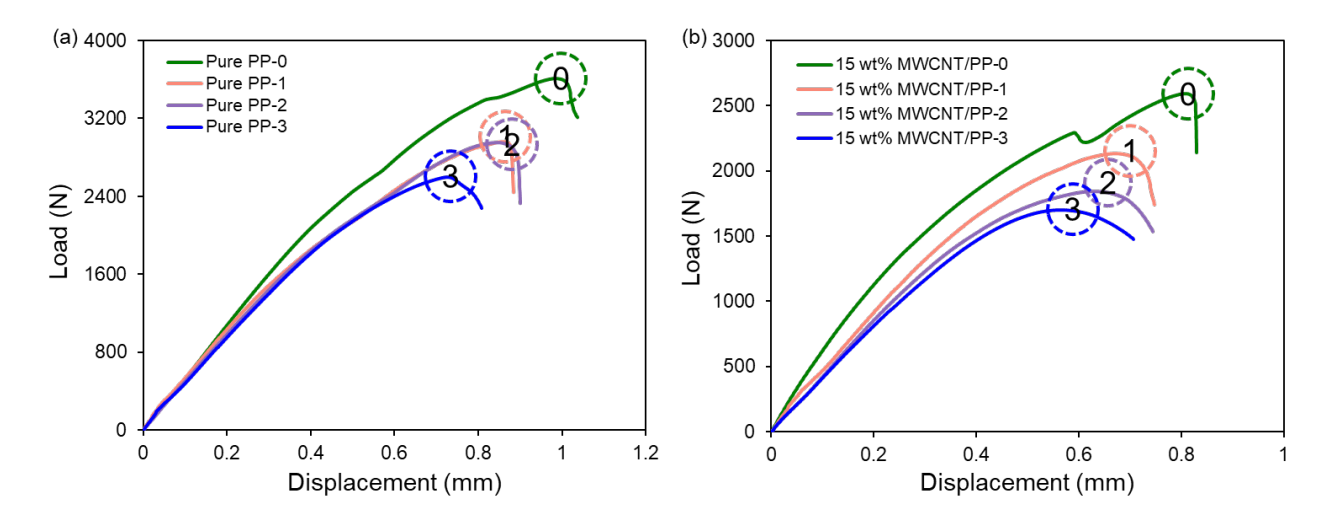


Figure 4. Representative load-displacement curves for repaired specimens after each repair cycle: (a) pure PP-GF/PP and (b) MWCNT-GF/PP SLJs. The numbers (0, 1, 2, and 3) indicate the number of the repair cycles and dashed circles indicate the position of peaks in the load curves.

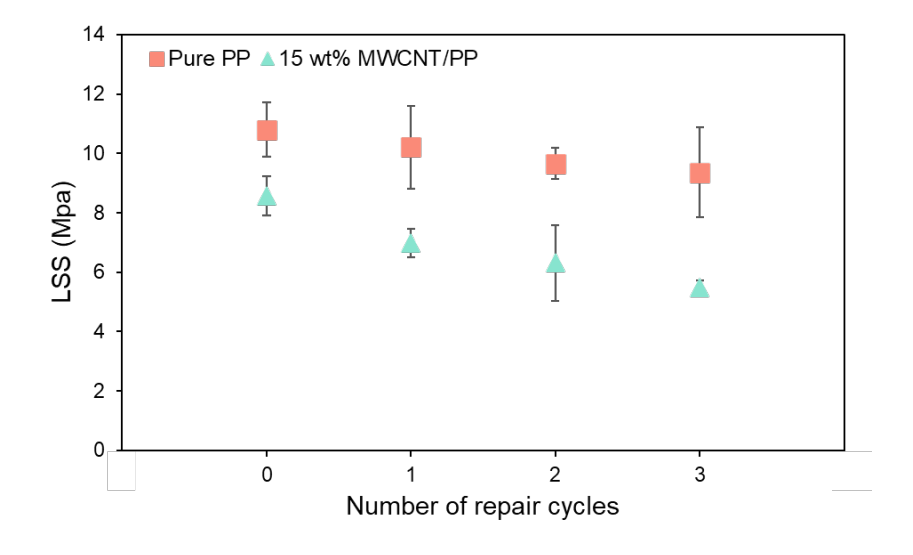


Figure 5. The effect of repair cycles on the LSS of GF/PP joints.

3.2. Failure mode analysis of repaired joints

The different tensile behavior of repaired PP and MWCNT/PP SLJs can be explained by the macro/micro-structural changes at the welding interface. Visual inspection of the fracture surfaces between repair cycles (Figure 6 and Figure 7) displays more unmolten films (Figure 6c and Figure 7d) and broken fibers (Figure 6d) as repair cycles increase. Furthermore, fiber deformation is observed at the edge of the fractured surfaces (Figure 7c and d), which might accelerate the failure of MWCNT-GF/PP SLJs, compared to PP-GF/PP SLJs, and further contribute to their reduction in LSS. While interlaminar failure is present after each repair cycle, it is worth noting that interfacial failure (between unmolten ED and adherend) gradually becomes more important after the second and third repair cycles. Therefore, the combination of unmolten films, broken fibers, and fiber deformation likely give rise to the reduction in mechanical properties of repaired joints.

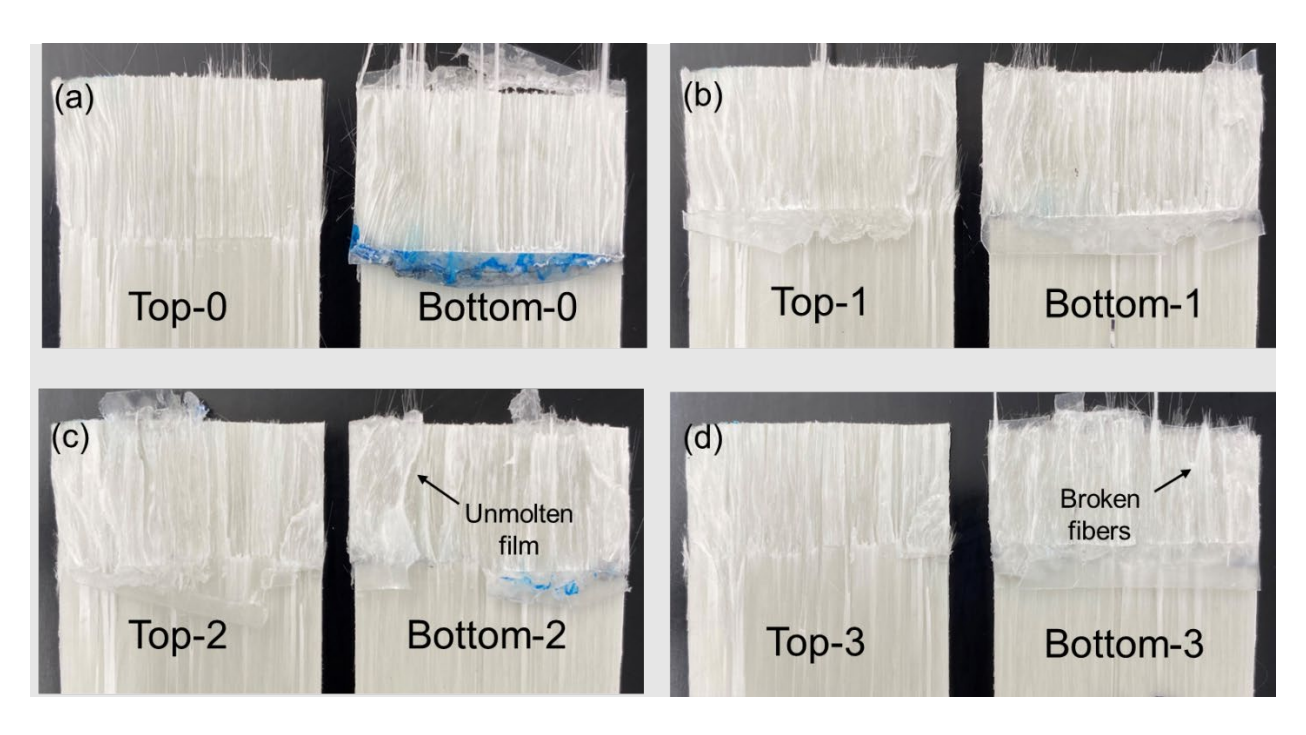


Figure 6. Fracture surface of PP-GF/PP SLJs after each repair cycle: (a) initial, (b) first, (c) second, and (d) third.

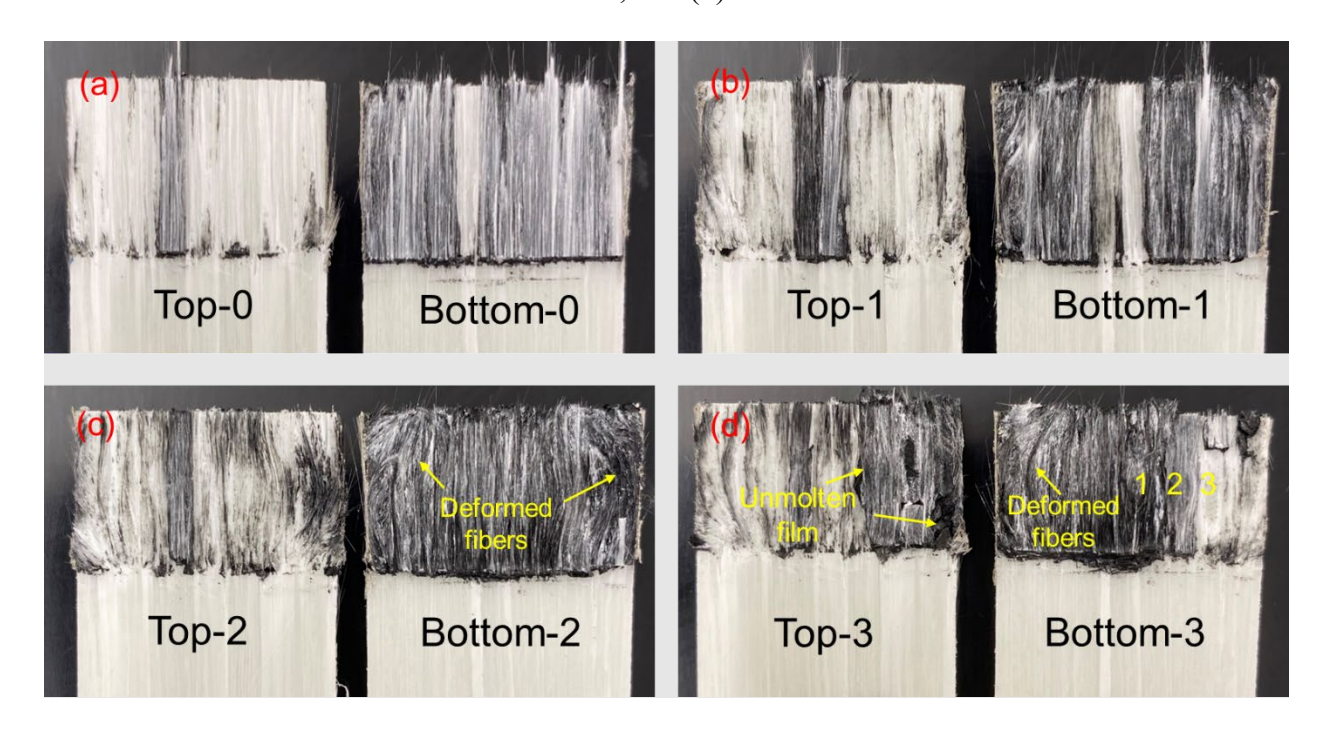


Figure 7. Fracture surface of MWCNT-GF/PP SLJs after each repair cycle: (a) initial, (b) first, (c) second, and (d) third.

Fractographic examinations provided a deeper understanding of the tensile behavior of repaired joints. Figure 8a and b present SEM images of the fracture surfaces for PP-GF/PP and MWCNT-

GF/PP SLJs after the third repair cycle, respectively. Different fracture patterns in the matrix can be seen in these two images. At the same magnification, the matrix in PP-GF/PP SLJs is more intact and smoother than it is in MWCNT-GF/PP SLJs, which confirms that PP films are more ductile, as mentioned in Section 3.1. After failure of the initial MWCNT-GF/PP SLJs (Figure 8c), some glass fibers are visibly broken. After the third repair cycle, the number of broken glass fibers increased from the previous cycles, shown in Figure 8d, corresponding to the reduced LSS from the initial case to the third repair cycle.

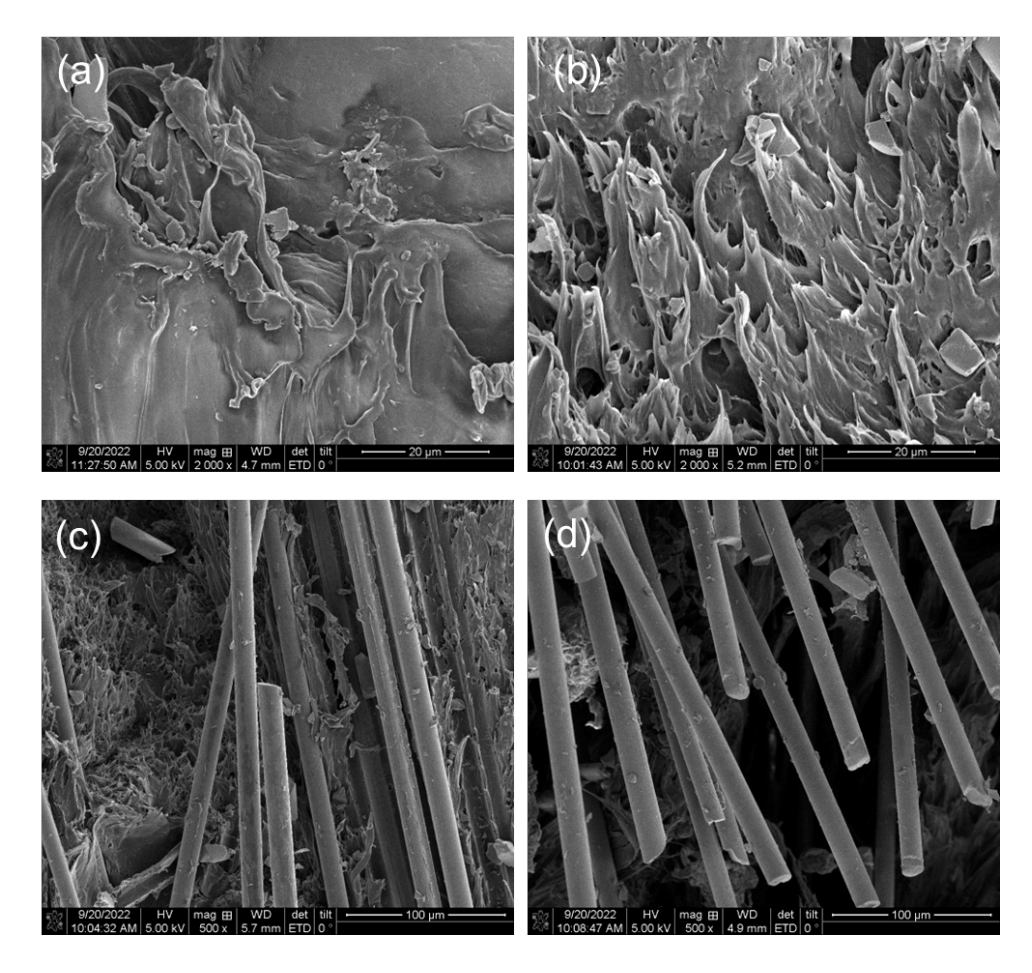


Figure 8. SEM images of fracture surfaces: (a) third repair cycle for PP-GF/PP, (b) third repair cycle for MWCNT-GF/PP, (c) initial MWCNT-GF/PP, and (d) third repair cycle for MWCNT-GF/PP SLJs.

3.3. Damage monitoring of repaired joints under tensile loading

Electrical resistance changes of MWCNT-GF/PP SLJs were captured during mechanical tests. Figure 9 presents the representative load and percentage change of electrical resistance for each repair cycle. In addition to the initial SLJs, the electrical resistance response of repaired SLJs (after the first cycle) displays typical characteristics as well. As shown in Figure 9b, at around 32 s, damage initiation occurs followed by a slight increase in resistance at step ①, indicating that some conductive pathways start breaking due to the increasing tensile loading. At the beginning of the tensile test, the percentage change of electrical resistance is almost flat due to the contacts between

MWCNTs without damage initiation. However, as damage accumulates, more and more conductive channels break, leading to an exponential increase in resistance (between step (2) and step (3)). Subsequently, electrical resistance jumps to infinity when the joint fully breaks under loading. This load and electrical resistance response is consistent with our previous study on SLJs welded with MWCNT-based nanocomposite films subjected to tension [24]. Furthermore, nanocomposite films still present high sensitivity with an infinite value in resistance after the first repair operation. The overall change in electrical resistance of the second and third repaired SLJs is relatively small, less than 10 %. On the other hand, there is more noise in electrical resistance data after the second and third repair cycles, especially in Figure 9d. This phenomenon may correspond to the unmolten nanocomposite film (Figure 7d), the significant fracture patterns (Figure 7d 1, 2, and 3), or less uniform distribution of conductive paths, which are confirmed in Figure 10b, c, and d. Nonetheless, a sudden increase in resistance can be seen when load drops (Figure 9c and d). However, it is noteworthy, that the resistance for the second and third repaired SLJs does not increase toward infinity, indicating that some connections still exist between MWCNTs even after the tests have been completed. This is likely due to the large number of conductive networks created by the successive use of nanocomposite films at the interface for the repair process.

Overall, each noticeable drop in load is always accompanied by a sharp jump in resistance. The graphs of load and electrical resistance response indicate that this nanocomposite-based in-situ monitoring technique has potential to monitor the initiation and propagation of damage in the weld line of repaired TPC SLJs, although its sensitivity seems to decrease with repair cycle.

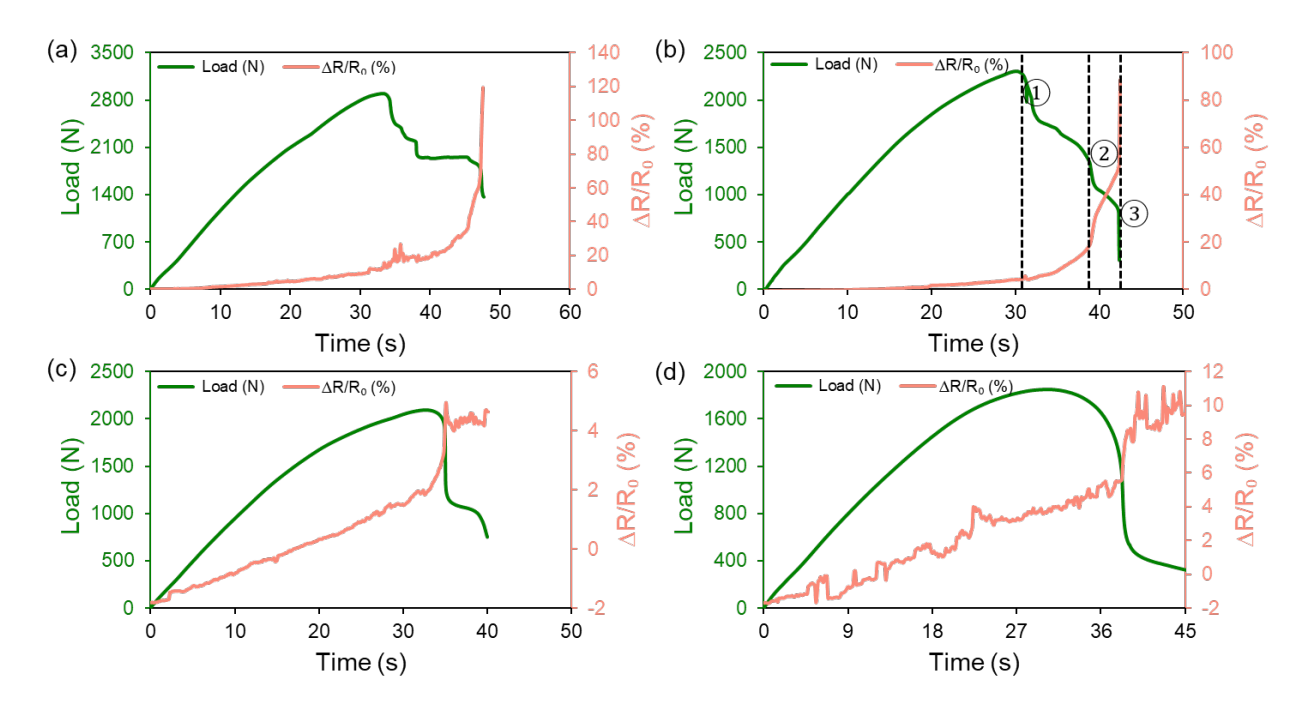


Figure 9. Load and percentage change of electrical resistance curves during tensile tests for MWCNT-GF/PP SLJs with different repair cycles: (a) initial, (b) first, (c) second, and (d) third.

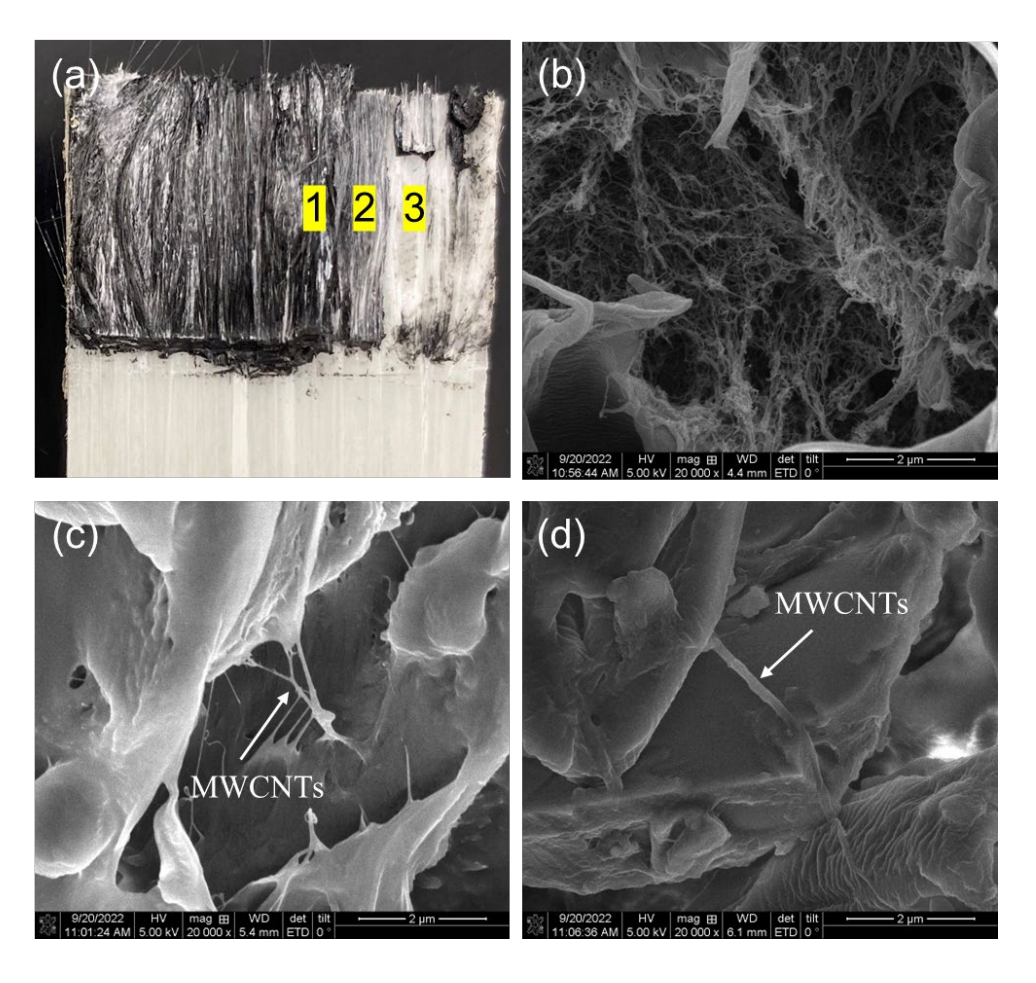


Figure 10. (a) Fracture surface after the third repair cycle and corresponding SEM images for MWCNT-GF/PP SLJs: (b) position 1 in (a), (c) position 2 in (a), and (d) position 3 in (a).

4. CONCLUSIONS

This work explored an ultrasonic-assisted technique for successively repairing thermoplastic composite joints (three cycles) with two types of films: pure PP and MWCNT/PP films. Tensile tests were performed to assess the ability of this repair technique in restoring mechanical properties while monitoring damage using electrical resistance measurements. Based on the experimental outcomes, the following observations were made:

- Ultrasonic-assisted repair using nanocomposite films was partially effective in recovering the strength of GF/PP SLJs. After each repair cycle, 94.5 %, 89.4 %, and 86.7 % LSS recovery was obtained for PP films and 81.3 %, 73.6 %, and 63.8 % for MWCNT/PP films with respect to the initial joint.
- Fractographic analysis revealed that failure modes changed with repair cycles, and the macro/micro-structural changes had a significant effect on the mechanical properties of repaired GF/PP joints and the electro-mechanical response under tensile loading.
- Nanocomposite films developed in this study hold promise for examining the initiation and propagation of damage within ultrasonically repaired thermoplastic composite joints, even after three repair cycles.

Future work will focus on improving repair effectiveness of the ultrasonic-assisted technique for thermoplastic composites through rewelding broken joints with different travel value or repairing joints using resistance heating and pressure. Furthermore, the incorporation of plasticizers through solvent dispersion to reduce the brittleness of nanocomposite films and then improve the mechanical properties while maintaining their electrical conductivity, will be explored.

5. ACKNOWLEDGMENTS

This work was supported by the National Science Foundation CAREER award (CMMI, Advanced Manufacturing, Award #2045955); the Louisiana Board of Regents under the Research Competitiveness Subprogram (contract number LEQSF (2018–2023)-RD-A-05); and the LSU Graduate School Economic Development Assistantship.

6. REFERENCES

- 1. Yu X., Fan Z., Puliyakote S., and Castaings M. "Remote monitoring of bond line defects between a composite panel and a stiffener using distributed piezoelectric sensors." Smart Materials and Structures 27(3) (2018): 035014. 10.1088/1361-665X/aaa69b
- 2. Sahoo C. K., Bhatia G. S., and Arockiarajan A. "Effect of patch-parent stacking sequence and patch stiffness on the tensile behaviour of the patch repaired carbon-glass hybrid composite." Thin-Walled Structures 179 (2022): 109551. 10.1016/j.tws.2022.109551
- 3. Khashaba U. A., and Najjar I. M. R. "Adhesive layer analysis for scarf bonded joint in CFRE composites modified with MWCNTs under tensile and fatigue loads." Composite Structures 184 (2018): 411-427. 10.1016/j.compstruct.2017.09.095
- 4. Ji X., Zhou W., Sun H., Liu J., and Ma L.-h. "Damage evolution behavior of bi-adhesive repaired composites under bending load by acoustic emission and micro-CT." Composite Structures 279 (2022): 114742. 10.1016/j.compstruct.2021.114742
- 5. Rito R. L., Crocombe A. D., and Ogin S. L. "Health monitoring of composite patch repairs using CFBG sensors: Experimental study and numerical modelling." Composites Part A: Applied Science and Manufacturing 100 (2017): 255-268. 10.1016/j.compositesa.2017.05.012
- 6. Cao D., Hu H., Wang Y., and Li S. "Experimental and numerical studies on influence of impact damage and simple bolt repair on compressive failure of composite laminates." Composite Structures 275 (2021): 114491. 10.1016/j.compstruct.2021.114491
- 7. Loh T. W., Ladani R. B., Ravindran A., Das R., Kandare E., and Mouritz A. P. "Z-Pinned composites with combined delamination toughness and delamination Self-Repair properties." Composites Part A: Applied Science and Manufacturing 149 (2021): 106566. 10.1016/j.compositesa.2021.106566
- 8. Bhatia G. S., and Arockiarajan A. "Fatigue studies on patch repaired carbon/epoxy woven composites." Composites Part B: Engineering 175 (2019): 107121. 10.1016/j.compositesb.2019.107121
- 9. Hall Z. E. C., Liu J., Brooks R. A., Liu H., Crocker J. W. M., Joesbury A. M., Harper L. T., Blackman B. R. K., Kinloch A. J., and Dear J. P. "The effectiveness of patch repairs to restore the impact properties of carbon-fibre reinforced-plastic composites." Engineering Fracture Mechanics 270 (2022): 108570. 10.1016/j.engfracmech.2022.108570

- 10. Zhou W., Ji X.-l., Yang S., Liu J., and Ma L.-h. "Review on the performance improvements and non-destructive testing of patches repaired composites." Composite Structures 263 (2021): 113659. 10.1016/j.compstruct.2021.113659
- 11. Loh T. W., Ladani R. B., Orifici A., and Kandare E. "Ultra-tough and in-situ repairable carbon/epoxy composite with EMAA." Composites Part A: Applied Science and Manufacturing 143 (2021): 106206. 10.1016/j.compositesa.2020.106206
- 12. Li G., Ji G., and Zhenyu O. "Adhesively bonded healable composite joint." International Journal of Adhesion and Adhesives 35 (2012): 59-67. 10.1016/j.ijadhadh.2012.02.004
- 13. Barroeta Robles J., Guthrie A., Dubé M., Hubert P., and Yousefpour A. "An approach to the repair of thermoplastic composites using resistance welding with a hybrid heating element". SAMPE Conference Proceedings. Charlotte, NC, May 23-26, 2022. Society for the Advancement of Material and Process Engineering pp.
- 14. Jongbloed B., Teuwen J., Benedictus R., and Villegas I. F. "On differences and similarities between static and continuous ultrasonic welding of thermoplastic composites." Composites Part B: Engineering 203 (2020): 108466. 10.1016/j.compositesb.2020.108466
- 15. Jongbloed B., Vinod R., Teuwen J., Benedictus R., and Villegas I. F. "Improving the quality of continuous ultrasonically welded thermoplastic composite joints by adding a consolidator to the welding setup." Composites Part A: Applied Science and Manufacturing 155 (2022): 106808. 10.1016/j.compositesa.2022.106808
- 16. Köhler F., Villegas I. F., Dransfeld C., and Herrmann A. "Static ultrasonic welding of carbon fibre unidirectional thermoplastic materials and the influence of heat generation and heat transfer." Journal of Composite Materials 55(15) (2021): 2087-2102. 10.1177/0021998320976818
- 17. Palardy G., Shi H., Levy A., Le Corre S., and Fernandez Villegas I. "A study on amplitude transmission in ultrasonic welding of thermoplastic composites." Composites Part A: Applied Science and Manufacturing 113 (2018): 339-349. 10.1016/j.compositesa.2018.07.033
- 18. Tsiangou E., Kupski J., Teixeira de Freitas S., Benedictus R., and Villegas I. F. "On the sensitivity of ultrasonic welding of epoxy- to polyetheretherketone (PEEK)-based composites to the heating time during the welding process." Composites Part A: Applied Science and Manufacturing 144 (2021): 106334. 10.1016/j.compositesa.2021.106334
- 19. Tsiangou E., Teixeira de Freitas S., Fernandez Villegas I., and Benedictus R. "Investigation on energy director-less ultrasonic welding of polyetherimide (PEI)- to epoxy-based composites." Composites Part B: Engineering 173 (2019): 107014. 10.1016/j.compositesb.2019.107014
- 20. Zhao T., Rans C., Fernandez Villegas I., and Benedictus R. "On sequential ultrasonic spot welding as an alternative to mechanical fastening in thermoplastic composite assemblies: A study on single-column multi-row single-lap shear joints." Composites Part A: Applied Science and Manufacturing 120 (2019): 1-11. 10.1016/j.compositesa.2019.02.013
- 21. Barroeta Robles J., Dubé M., Hubert P., and Yousefpour A. "Repair of thermoplastic composites: an overview." Advanced Manufacturing: Polymer & Composites Science 8(2) (2022): 68-96. 10.1080/20550340.2022.2057137
- 22. Frederick H., Li W., and Palardy G. "Disassembly Study of Ultrasonically Welded Thermoplastic Composite Joints via Resistance Heating." Materials 14(10) (2021): 2521. 10.3390/ma14102521

- 23. Frederick H., Li W., Sands W., Tsai E., and Palardy G. "Multifunctional films for fusion bonding and structural health monitoring of thermoplastic composite joints". SAMPE Conference Proceedings. Virtual, 4-7 May, 2020. Society for the Advancement of Material and Process Engineering. pp.
- 24. Li W., Frederick H., and Palardy G. "Multifunctional films for thermoplastic composite joints: Ultrasonic welding and damage detection under tension loading." Composites Part A: Applied Science and Manufacturing 141 (2021): 106221. 10.1016/j.compositesa.2020.106221
- 25. Li W., and Palardy G. "Mechanical/electrical properties of MWCNT/PP films for structural health monitoring of GF/PP joints". ACCE Conference. Novi, MI, 2-4 November, 2021. SPE Automotive and Composites Divisions. pp.
- 26. Li W., and Palardy G. "Electro-Mechanical Response of Ultrasonically Welded Thermoplastic Composite Interfaces under Static and Cyclic Flexural Loads Using Nanocomposites." ACS Applied Polymer Materials 4(7) (2022): 5209–5223. 10.1021/acsapm.2c00737
- 27. Li W., and Palardy G. "Damage monitoring methods for fiber-reinforced polymer joints: A review." Composite Structures 299 (2022): 116043. 10.1016/j.compstruct.2022.116043
- 28. Farahani R. D., and Dubé M. "Novel heating elements for induction welding of carbon fiber/Polyphenylene sulfide thermoplastic composites." Advanced Engineering Materials 19(11) (2017): 1700294. 10.1002/adem.201700294
- 29. Farahani R. D., Janier M., and Dube M. "Conductive films of silver nanoparticles as novel susceptors for induction welding of thermoplastic composites." Nanotechnology 29(12) (2018): 125701. 10.1088/1361-6528/aaa93c